May 2017

Performance Test of the Pasquill Stability Classification Scheme

Hillary Lin Chapman
University of Wisconsin-Milwaukee

PERFORMANCE TEST OF THE PASQUILL STABILITY CLASSIFICATION SCHEME

by

Hillary Chapman

A Thesis Submitted in

Partial Fulfillment of the

Requirements for the Degree of

Master of Science

in Mathematics

at

The University of Wisconsin-Milwaukee

May 2017

ABSTRACT

PERFORMANCE TEST OF THE PASQUILL STABILITY CLASSIFICATION SCHEME

by

Hillary Chapman

The University of Wisconsin-Milwaukee, 2017
Under the Supervision of Professor Jon Kahl

In 1961, Frank Pasquill proposed a method for classifying atmospheric stability based on routinely available surface observations – namely wind speed, cloud cover, and the strength of incoming solar radiation. Stability is classified into six categories: extremely unstable (A); moderately unstable (B); slightly unstable (C); neutral (D); slightly stable (E); and moderately stable (F). These categories are ultimately meant to be used to determine the rate of diffusion of windblown pollutants, but since their inception, the classes have often seen use outside of their originally intended purpose. In this thesis, the performance of the Pasquill scheme is tested in order to determine whether it is appropriate to use it in a non-diffusion related setting. Stability derived using the Pasquill stability scheme is compared to stability derived from temperature lapse rates, using surface and upper air data obtained from the NOAA NCEI for six sites across the Eurasian continent for the years 2000-2010. The Pasquill scheme is found to be biased towards neutral stability, with 57% of all cases determined to be class D – but the actual surface-100m temperature lapse rates were found to be biased towards stable conditions, with 70% of all cases falling into the stable stability range. The Pasquill scheme did perform best under stable conditions, with over 90% the E and F classes occurring when stable conditions were actually

present. However, the scheme performed poorly during unstable conditions, correctly predicting an unstable class in only 57% of all unstable cases. The Pasquill method performed the worst under neutral conditions, correctly with neutral conditions present for only 5% of the cases when class D was predicted.

TABLE OF CONTENTS

LIST OF FIGURES

LIST OF TABLES

I. Introduction

Before the accident at Chernobyl, the worst nuclear disaster in European history occurred on October 10th, 1957 – when, as Leatherdale (2010) explains, a fire broke out in one of the reactors of the Windscale plutonium production plant in the county of Cumbria, United Kingdom. Clad in radiation suits, the firefighters could only battle the flames for up to three hours at a time with such high radiation levels, and Leatherdale (2010) mentions that they were only able to finally put out the fire by cutting off the air to the reactor room. With radioactive material spreading across the UK and Europe, the British Meteorological Office was tasked with creating a procedure to calculate the concentrations of windborne material downwind of an emitting source at the surface, using routinely available surface data (Pasquill and Smith, 1983).

Frank Pasquill developed a method for obtaining estimates of the vertical and crosswind spread of windborne material for distances up to 100 km downwind from the source, given stability categories based on surface observations of wind speed, incoming solar radiation, and sky cover. These stability categories range from A (extremely unstable) to F (moderately stable), with D being the neutral category (Table 1, 2). These classes are used to stratify atmospheric diffusion data into stability-dependent curves (Figures 1 and 2) describing the vertical and crosswind spread of a plume downwind of an emitting source. These curves can then be used in conjunction with the Gaussian plume equation to finally provide an estimate of pollutant concentration (e.g. Hanna, et al 2001).

Table 1: The Pasquill stability classes and their corresponding stability type. From Pasquill (1961).

A: Extremely unstable conditions	D: Neutral conditions
B: Moderately unstable conditions	E: Slightly stable conditions
C: Slightly unstable conditions	F: Moderately stable conditions

Table 2. Method of choosing each Pasquill stability class based on surface wind speed and sky conditions. From Pasquill (1961).

	Daytime insolation			Night-Time Conditions	
Surface wind speed (m/s)	Strong	Moderate	Slight	Thin overcast or > 4/8 low cloud	<= 4/8 cloudiness
< 2	A	A - B	B	E	F
2 - 3	A - B	B	C	E	F
3 - 5	B	B - C	C	D	E
5 - 6	C	C - D	D	D	D
> 6	C	D	D	D	D

The Pasquill stability scheme is only one of a number of methods used to determine pollutant concentrations, and several studies have compared the effectiveness of the Pasquill scheme against these other methods. Vertical radon-concentration gradients are used by Crawford, et al (2016) and Chambers, et al (2015) to determine stability, and when estimates of pollutant concentrations using this stability scheme are compared to estimates derived from the Pasquill stability classes, both studies find that the Pasquill stability scheme under-predicted pollutant concentrations under stable conditions. Koehn, et al (2013) uses the stability classes in one of three different dispersion model runs to calculate the emission rates of ammonia and methane, and find that the model run using stability determined via the Pasquill stability categories was outperformed by two others that used a sonic anemometer and the gradient Richardson number to estimate stability. Mohan and Siddiqui (1998) and Luna and Church (1972) compare several different stability schemes in order to determine which best represents the diffusion capability of the atmosphere for a given location, and found that there is a wide

range of stability types possible for the different surface wind and sky conditions corresponding to each individual Pasquill stability class. The performance of the stability classes has also been compared to other methods in areas with more complex terrain. Erbrink and Scholten (1995) evaluate the performance of the Pasquill stability scheme near a coastline, noting that estimates of stability matched up well with the stable cases overland. Wang (1992) uses the classes to determine pollutant concentrations in the city of Lanzhou, China, which is located in a river valley and surrounded by mountains, and finds large differences between other estimates of stability and the Pasquill stability classes.

The Pasquill stability classes were used in these studies for the originally intended purpose of estimating pollutant concentrations downwind of a source. However, the Pasquill stability classes have also been used in many additional studies simply to classify the actual atmospheric stability – and not ultimately to determine pollutant concentrations. Krueger and Emmanuel (2013); Tomlinson, et al (2012); and Mohan, et al (2012) use the Pasquill stability classes while studying urban heat islands. Chapman, et al (2001) use the stability classes to model road surface temperatures given a certain type of stability. No and Kim (2005) use the stability classes to simulate outdoor conditions in a study on the performance of curtain walls in high-rise structures. G.P Van den Berg (2003, 2005) uses the classes in his investigations on wind farm noise and atmospheric stability. The size of spore clusters has been evaluated, under certain weather conditions corresponding to the different stability classes, by Handler and Edwards (2015). Stability is determined via the Pasquill stability classes to characterize the nocturnal boundary layer by Kim, et al (2000) and Kurzeja et al (1990). Sempreviva, et al (1994) use the Pasquill stability classes to test the European Environmental Commission's wind climatology model in areas along the Mediterranean Coast. Serizawa et al (1992) use the Pasquill

scheme to determine atmospheric stability conditions and forecast the occurrence of fading in microwave radio circuits. Duenas et al (1994) find estimates of stability via the Pasquill scheme in their study on the use of radon daughters as an atmospheric tracer given certain stability conditions. Finally, Masters, et al (2010), in their study of terrain impacts on observed wind gust data standardization, determined atmospheric stability using the Pasquill scheme and excluded gust factors observed during non-neutral conditions from their study.

These studies fall outside of the scope of atmospheric diffusion, so why use the Pasquill scheme at all? Surface data necessary to obtain a Pasquill stability class are usually available for any site of interest – which was, after all the point of the classes in the first place. This means that this scheme provides a more convenient method of characterizing atmospheric stability than methods involving, for example, vertical radon concentrations, Richardson numbers, sonic anemometers, or temperature lapse rates, which necessitate the use of special equipment or upper air data that are not available as frequently or at as many locations as surface observations.

The accuracy of the Pasquill stability classes for more general use (not involving atmospheric diffusion) has not been tested. In this thesis, the Pasquill scheme will be compared to stability estimates derived from the environmental temperature lapse rate, which is commonly used to determine stability and atmospheric buoyancy. These comparisons will be used to assess the ability of the Pasquill scheme to characterize atmospheric stability independent of its originally intended purpose.

II. Data and Methods

a. Description of sites chosen

Surface and upper air data are obtained from the NOAA National Centers for Environmental Information (NCEI) for six sites spanning the Eurasian continent for the years 2000-2010. These sited include Merignac, France, located near Bordeaux in the southwestern portion of the country; Kiev, Ukraine; Makhachkala, Russia, on the Caspian Sea; Taraz, in southern Kazakhstan near the border of Kyrgyzstan; Ulaanbaatar, in northeastern Mongolia; and Poronaysk, Russia, on the eastern side of Sakhalin Island on the Sea of Okhotsk. Figure 3 shows the six sites indicated with markers on a map of Eurasia, and Table 3 contains information about these sites.

Table 3. Table of information on the six sites used.

Site	Latitude $°N$	Longitude $°E$	Surface Elevation (msl)	Time Zone
1. Merignac	44.83	-0.70	61	UTC +1
2. Kiev	50.40	30.56	167	UTC +2
3. Makhachkala	43.01	47.01	-21	UTC +3
4. Taraz	42.85	71.38	651	UTC +6
5. Ulaanbaatar	47.55	106.52	1306	UTC +8
6. Poronaysk	49.22	143.10	4.0	UTC +11

These sites were selected based on the following criteria: they were co-located surface and upper-air observation stations; surface and upper-air data were available for the entire period of interest, with gaps in the data spanning no longer than several weeks; they all fell within a similar range of latitudes, around 40-50 degrees; they were spaced longitudinally so as to allow for sampling of a wide range of stabilities. This last criterion has to do with the fact that radiosonde data is collected only twice daily, at 0Z and 12Z. At Merignac, this would correspond to 1am and 1pm, but at Taraz, for example, these times correspond to 6am and 6pm. This would

often result in stable (unstable) conditions at Merignac at 0Z (12Z), and stable (neutral) conditions at 0Z (12Z) for Taraz.

b. Surface Data and Calculating the Pasquill Stability Class

Surface observations necessary to calculate the Pasquill stability class include wind speed, as well as sky cover and ceiling height to determine the strength of insolation. An observation is therefore discarded if wind speed, sky cover, or ceiling height is missing. The method for determining insolation in this study is adapted from Luna and Church (1972). First, the solar elevation angle (sun angle) is determined. This is found by first calculating the day number (1-365, or 366 in a leap year). The hour angle (h) is calculated next, using the following equation from Stull (1988):

$$\text{h} = \pi \times \frac{t_{utc}}{12} \text{ - longitude} \quad (1)$$

where t_{utc} is the observation time in UTC. Next, the declination angle (δ) is determined, using:

$$\delta = .409 \times \cos \frac{Julian\ day\ number - 173}{365.25} \quad (2)$$

The hour angle and declination angle are used to find the solar elevation angle (ψ) in the following way:

$$\sin(\psi) = \sin(latitude) \times \sin \delta - \cos(latitude) \times \cos \delta \times \cos h \quad (3)$$

Taking the arcsine and converting to degrees gives the solar elevation angle in degrees. The strength of insolation for different sun angles are described in Table 4.

Table 4. Strength of Insolation in terms of the sun angle. From Luna and Church (1972).

Insolation Strength	Insolation Code	Sun Angle (Degrees)
Strong	3	>60
Moderate	2	35-60
Slight	1	15-35
None	0	0-15
Night	-2	0

After calculating the sun angle, the corresponding insolation code in Table 4 is designated as the clear-sky insolation code. To determine the impacts of clouds, a cloud modifier code is found next, using Table 5.

Table 5. Cloud Modifier Code. Determined by total coverage and cloud height. From Luna and Church (1972).

Description	Sky Condition	Total amounts (tenths)	Amount (tenths)	Cloud Type	Height (100's feet)	Cloud Modifier Code
Clear to Scattered		0-5				21
High thin overcast	Thin overcast	10		Ci, Cs, Cc	>180	22
Broken Middle		6-9	6-9	Ac, Acc, As, Ns	60-180	23
Broken Low		6-9	6-9	F, St, Sc, Cu, Cb	<60	24
Overcast		10				25

A cloud modifier code of 21 would mean that clouds do not impact the strength of insolation, while cloud codes of 22-25 mean that clouds result in a reduced strength of insolation. Once the cloud modifier code is identified, it is used with the clear-sky insolation code to determine the final insolation code (Table 6).

Table 6. Final Insolation Code, based on the Clear Sky Insolation Code and the Cloud Modifier Code. From Luna and Church (1972).

Cloud Modifier Code	Clear Sky Insolation Code				
	-2	**0**	**1**	**2**	**3**
21	-2	0	1	2	3
22	-2	0	1	1	2
23	-2	0	0	1	2
24	0	0	0	0	1
25	0	0	0	0	0

The insolation code determined in the previous step corresponds to the categories defined in Table 4 (Strong, Moderate, etc), but this time the effects of clouds have been added. This

insolation code is used with the wind speed in Table 2 to find the Pasquill Stability Class. The classes are numbered 1 (A) through 6 (F) for the purposes of future comparison to the upper air data. When the insolation is Moderate or Strong, there are several cases where one of two stability classes is possible for the given range of wind speeds. In these cases, if the wind speed is closer to the higher (lower) end of the given range, the more stable (unstable) class is chosen. An example of the above process for a sample surface observation with a wind speed of 3m/s, a ceiling height of 7000 ft., 7/10 sky cover and a solar elevation angle of 40° is as follows: the clear-sky insolation code of 2 is determined from Table 4. A cloud modifier code of 23 is obtained from Table 5. A final insolation code of 1 is obtained from Table 6. This final insolation code is inserted into Table 4 once again, and corresponds to the "slight" daytime insolation category. "Slight" insolation and an observed wind speed of 3m/s are conditions corresponding to Pasquill Class C, slightly unstable conditions.

c. Upper air data and calculating temperature lapse rates

Upper air data is obtained from the NCEI for 2000-2010, and then divided into 2000-December 2004 and 2005-December 2010 blocks for ease of calculation. The data used in this study include temperature, geopotential height, and pressure. First, the sounding files are checked for missing data in the pressure, height, and temperature fields. When these data are missing, they need to be estimated using the hydrostatic and hypsometric equations, but this means that any sounding level that has more than one of these fields missing cannot be used. When pressure alone is missing, it is calculated using the hypsometric equation as follows:

$$p_1 = p_2 \times e^{\frac{2 \times g \times (z_2 - z_1)}{R_d \times (T_2 + T_1)}} \quad (4)$$

where p_1, T_1 and p_2, T_2 are the pressures and temperatures at altitude $z_1$and z_2, respectively; R_d, g are the specific gas constant for dry air and the acceleration due to gravity, respectively.

Density is calculated for every level of each sounding (for which temperature and pressure available). Then, for every level where height is missing, it is calculated with the hydrostatic equation as follows:

$$z_2 = z_1 - \frac{p_2 - p_1}{\rho g} \quad (5)$$

Finally, when the temperature at a sounding level is missing, it is calculated by using the hypsometric equation as follows:

$$T_1 = \frac{2 \times g \times (z_2 - z_1)}{R_d \times \ln \frac{p_1}{p_2}} - T_2 \quad (6)$$

With all missing data on usable sounding levels filled in, each sounding is then broken up into surface-to-100m, surface-to-200m, surface-to-300m, surface-to-400m, and surface-to-500m layers. However, there is rarely a sounding level exactly at 100m, 200m, 300m, 400m, or 500m, so the final level of each of the layers mentioned above is actually the first level reported above the altitude of interest. The temperature at the altitude of interest is found by linear interpolation, using the temperature at the last altitude below and first altitude above this level. Sample soundings for every site after this step are shown in Figures 4-9. These figures, the original soundings overlaid with the interpolated 100m-500m temperature, show that, as would be expected, the temperature at each of these altitudes falls along the temperature profile line connecting all of the actual observed temperatures in the original soundings. There is another detail indicated by the sample temperature profiles from Figures 4-9: not all of the original soundings even from this small, two-observation sample contain the same number of levels. For example, the Merignac, FR sounding for 1/5/04 at 0Z (Figure 4) originally contained seven levels, while the sounding from Kiev, UA at the same time (Figure 5) contained only two levels.

The soundings utilized have already been subjected to quality-control procedures, but additional quality-control checks are applied in this study in order to ensure that the temperatures

calculated using the original data are accurate. The average temperature for all January-December for each 2000-2004 and 2005-2010 block is calculated. For every level for which the temperature had to be calculated, the level is only included in further calculations if this temperature falls within +/- three standard deviations of the average temperature for that month.

Once the temperature at the altitude of interest has been estimated, lapse rates are calculated between every level of the five different layers of each sounding, using:

$$\Gamma = \frac{-\Delta T}{\Delta z} \tag{7}$$

This results in multiple lapse rate estimates for every surface-to-x00 layer for every sounding. In order to find a single lapse rate estimate for every surface-to-x00 layer, and therefore five estimates of the temperature lapse rate for every sounding, an average lapse is found for every layer, weighted against the thickness of the layer over which every lapse rate was taken:

$$\Gamma_{sfc-x00} = \frac{\sum_{i=2}^{n} \Gamma_i \times d_i}{\sum_{i=2}^{n} d_i} \tag{8}$$

where n is the number of levels in every surface-to-x00 layer, Γ_i is the environmental lapse rate within the sublayer bounded by

$$d_i = z_i - z_{i-1} \tag{9}$$

The number of levels in every surface-to-x00 layer is also retained. Upper air data is then combined into full ten-year sets, but divided into separate 0z and 12z subsets.

For a final layer of error-checking, each average temperature lapse rate is checked to determine whether it falls within three standard deviations of the monthly average sfc-x00m temperature lapse rate for all January-December for 2000-2010.

Finally, the lapse rates for each layer are divided into classes for comparison with the Pasquill stability categories. The ranges of lapse rates defining these classes were determined

following a comprehensive yet subjective examination of the observed lapse rates at the sounding sites utilized. Lapse rates that fall within $9.81℃/km \pm .5℃/km$ are classified as neutral (class D) or a score of 4. Temperature lapse rates below zero correspond to moderately stable conditions (class F) or a score of 6. Positive temperature lapse rates that are still less than the neutral temperature lapse rate correspond to slightly stable conditions (class E) or a score of 5. To determine how the unstable classes should be defined, histograms of the temperuatre lapse rates are examine. Sample histograms are provided in Figures 10 (for Merignac) and 11 (for Kiev). In the 12z soundings, corresponding to early afternoon at these two sites and stability conditions likely corresponding to slightly or moderately unstable, a peak in the number of lapse rates occurs at around 12-14 $℃/km$, then the number gradually falls back until around 20-22 $℃/km$, with a more rapid decline in the number of observed lapse rates higher than this. Similar results were shown for other sites, and for other levels. These ranges informed the choice of the thresholds for the unstable classes. Slightly unstable conditions (class C and score 3) correspond to temperature lapse rates between the neutral lapse rate and $13℃/km$. Moderately unstable conditions (class B and score 2) correspond to temperature lapse rates greater than or equal to $13℃/km$ but less than 20 $℃/km$. Extremely unstable conditions (class A and score 1) correspond to temperature lapse rates greater than or equal to 20 $℃/km$.

There is a concern that the results may be sensitive to the thresholds chosen to categorize the lapse rates into different types of stability. In order to determine the impact that this has on the results, a subset of the data, comprised of the soundings from Merignac, FR, is chosen to be categorized using different thresholds. Examining the 0z lapse rate histogram for Merignac, a majority of the data falls within the 6-9 $℃/km$ range, so it could be said that, for this site and time, the more extreme stability conditions were found below this range. Therefore, moderately

stable conditions are defined as a lapse rate less than $6℃/km$, and lapse rates between $6℃/km$ and the neutral lapse rate define slightly stable conditions. The thresholds defining the unstable categories are also adjusted. The moderately unstable class is chosen for lapse rates between $13℃/km$ and $16\ ℃/km$, and the extremely unstable class is chosen for lapse rates greater than $16\ ℃/km$. Upon examination, the change in thresholds causes a change in upper air stability class in approximately 20-45% of the 0z Merignac observations. A change in class occurs in approximately 11-28% of the 12z Merignac observations. However, there is never a change of more than one class, and the original set of thresholds (with a lower end of $0℃$ and a higher end of $20℃$) makes somewhat more sense meteorologically, as the lapse rates below $0℃$ occur in highly stable situations and lapse rates above $20℃$ are very rate in the data. Therefore, the original set of thresholds is used for the remainder of the study.

The dates for which the surface and upper air datasets overlap are determined, and the two datasets are combined. This further reduces the number of observations used in the analysis to 28,765 observations, as shown in Table 7.

Table 7. Number of initial surface and upper air observations, number of final surface and upper air observations, and number of observations for the overlapping dates for each site.

Site	Sfc, Initial	Upper, Initial	Sfc, Final	Upper, Final	Overlap
1	7989	6769	6159	6692	5124
2	7947	7211	5378	7020	4683
3	7920	5981	6427	5852	4622
4	7905	5268	6859	5204	4406
5	7988	7069	6427	6923	5500
6	7950	5183	6919	5119	4430

In order to test the performance of the Pasquill stability class against the "true" stability as determined by the upper air stability categories, a bias is calculated as follows, taking advantage of the fact that each stability class (A-F) has been assigned a number (1-6):

$$\text{Bias} = \text{Pasquill Stability Class} - \text{Upper Air Stability Class} \quad (10)$$

A small bias therefore corresponds to a closer match between the stability estimated using the Pasquill stability scheme, and that determined using the temperature lapse rates. A negative (positive) bias means that the Pasquill class is trending more unstable (stable) compared to the stability determined by the temperature lapse rates.

III. Results and Discussion

Histograms of the Pasquill Stability Categories determined for each site at 0z and 12z are shown in Figures 12-17. As expected, those times always corresponding to night time and early morning (like Merignac, Kiev, and Makhachkala at 0z) and afternoon (Merignac, Kiev, and Makhachkala at 12z) always have stability categories corresponding to neutral-stable (D-F) and unstable-neutral (A-D) conditions, respectively. The histograms for Taraz, Ulaanbaatar, and Poronaysk show a that a wider range of categories may be chosen for 0z or 12z, as these times correspond to later morning (Ulaanbaatar and Poronaysk at 0z) or early evening (Taraz at 12z). Depending on the time of year, the sun may be above the horizon at these times, which would result in a neutral to unstable category in the Pasquill scheme. However, it is clear from all of the histograms that the most frequently chosen stability category for all times and all sites is neutral, D (indicated by a number 4 in the histograms).

For comparison, the average and standard deviation is calculated for the bias and the absolute value of the bias for each sfc-x00 layer, for all 28,765 sites. These statistics are shown in Table 8 for the bias and Table 9 for the absolute value of the bias.

Table 8. Average and standard deviation of the bias for each layer, with N=28765.

	Sfc-100m Bias	Sfc-200m Bias	Sfc-300m Bias	Sfc-400m Bias	Sfc-500m Bias
Avg	-0.4	-0.5	-0.6	-0.7	-0.8
Std	1.4	1.3	1.2	1.2	1.1

Table 9. Average and standard deviation of the absolute value of the bias for each layer, with N=28765.

	Sfc-100m Abs(Bias)	Sfc-200m Abs(Bias)	Sfc-300m Abs(Bias)	Sfc-400m Abs(Bias)	Sfc-500m Abs(Bias)
Avg	1.2	1.1	1.1	1.1	1.1
Std	0.9	0.9	0.9	0.9	0.8

Judging from these tables alone, there is no easily defined relationship between the depth of the layer and the magnitude or sign of the bias – nor for the spread in the bias about the average for each layer. These values do show that, for the full dataset, the Pasquill stability class and the upper air stability class is separated by around one class on average (from Table 9) with a leading negative in the average bias values (Table 8) indicating that the Pasquill stability scheme generally trends toward a more unstable class when compared to the upper air stability class. An example of this would be a Pasquill stability class of E, slightly stable, determined when the upper air stability class is F, moderately stable. However, a standard deviation approaching and exceeding one class indicates that the Pasquill and upper air stability classes are also often separated by one or more classes. This would be a less-than-favorable situation, as it would mean that, for example, the Pasquill scheme could estimate the stability as neutral, D, when the "true" estimate stability (determined by the average temperature lapse rate over the layer) is moderately stable, F.

A signs test is performed to determine whether the difference between the five upper air stability classes and the Pasquill stability class is significant. For all five classes, the null hypothesis that there is no difference between the Pasquill stability classes and the upper air stability classes is rejected at the 99% confidence level.

In order to identify whether there are any other factors that impact the sign and magnitude of the bias, the bias for the full dataset is next stratified by month. Again, the average and standard deviation are calculated for each surface-x00m layer, and these statistics are shown in Table 10 for the surface-100m layer. This layer is chosen because most of the activities involved in the studies that featured uses of the Pasquill scheme for non-diffusion purposes would take place in this lowest layer of the atmosphere.

Table 10. Monthly average and standard deviation of the bias and absolute value of the bias, for the surface-100m layer at all sites and times.

Month	N	Bias	Std Bias	Abs(Bias)	Std Abs(Bias)
January	2426	-0.5	1.1	0.9	0.7
February	2128	-0.6	1.2	1.0	0.8
March	2374	-0.5	1.3	1.0	0.8
April	2280	-0.3	1.6	1.2	1.0
May	2467	-0.3	1.6	1.2	1.0
June	2391	-0.3	1.7	1.3	0.9
July	2545	-0.2	1.6	1.2	0.9
August	2476	-0.2	1.6	1.0	1.0
September	2337	-0.2	1.5	1.0	0.9
October	2539	-0.4	1.3	1.0	0.8
November	2393	-0.5	1.2	0.9	0.7
December	2411	-0.5	1.2	1.0	0.7

There appears to be a slight relationship between seasons and the magnitude of the bias. Again, the average bias is negative for all categories, indicating that the Pasquill stability scheme usually tends toward less stable conditions compared to the upper air stability classes every month. The average of the absolute value of the bias indicates that the two results are usually separated by at least one stability class, with the highest values in the spring through early fall. The standard deviation is largest during this period as well. A possible reason for this is the dependency of the Pasquill stability classification on the sun angle. When the sun is below the horizon, the Pasquill stability class is either neutral or a stable class – and when the sun is above the horizon, the class is always either neutral or an unstable class. For sites that have sounding launches during the early morning or early evening, like Taraz (at 12z) and Ulaanbaatar (at 0z), these sounding launches occur in daylight during the warmer months and in darkness during the late fall and winter. The histograms of the Pasquill stability classes at these two sites (shown in

Figure 13 and Figure 14, respectively) show that this results in a larger range of possible classes compared to the other sites.

In order to explore any possible relationship between the bias and the number of sounding levels within the layer over which the upper air stability class has been found, the data for the surface-100m layer is stratified according to the number of sounding levels present in each surface-100m layer. The average and standard deviation of the bias and absolute value of the bias are shown in Table 11.

Table 11. Average and standard deviation of the bias and absolute value of the bias, per number of sounding levels. Data from the surface-100m layer for all sites and times. Only one sounding (not shown) contained 6 levels.

Levels per Layer	N	Bias	Std Bias	Abs(Bias)	Std Abs(Bias)
2	17119	-0.5	1.3	1.1	0.9
3	10799	-0.3	1.6	1.3	1.0
4	1174	0.1	1.8	1.5	1.0
5	49	-0.6	1.4	1.1	1.1

The majority of the surface-100m layer lapse rates were calculated over a layer with 2-4 sounding levels. The bias is usually negative, again indicating that the Pasquill stability scheme trended more unstable compared to stability determined from the upper air data. The average bias moves closer to zero with an increasing number of levels over that 2-4 range, but then the bias becomes a larger negative again for those soundings with five levels. Over this range, the spread in the bias is largest when there are three or four levels per sounding. The absolute value of the bias is also largest for these two categories, and the standard deviation of the absolute value of the bias increases with an increasing number of sounding levels. Because there are fewer cases with a higher number of sounding levels for the surface-100m layer, it might be helpful to include statistics for a deeper layer. Table 12 contains the average and standard deviation of the bias for the surface-300m layer, stratified by the number of sounding levels.

Table 12. Average and standard deviation of the bias and absolute value of the bias, per number of sounding levels. Data from the surface-300m layer for all sites and times. Eight soundings (not shown) contained eight sounding levels, and three soundings (not shown) contained nine sounding levels.

Levels per Layer	N	Bias	Std Bias	Abs(Bias)	Std Abs(Bias)
2	1651	-0.6	1.0	1.0	0.6
3	14017	-0.6	1.2	1.1	0.8
4	10997	-0.6	1.3	1.1	0.9
5	2017	-1.1	1.3	1.2	1.1
6	215	-1.2	1.1	1.3	1.1
7	40	-1.0	1.2	1.0	1.2

The majority of the observations in the surface-300m layer occur when the number of levels per layer falls in the 2-5 layer range, then there is a small percentage with seven sounding levels. For the surface-100m layer data, the average bias moved closer to zero for layers with more levels. Conversely, the surface-300m bias actually becomes more negative with increasing number of sounding levels. The trend in the standard deviation data is in agreement with what was shown in Table 11: average absolute value of the bias and standard deviation increase with increasing number of levels for the categories containing the majority of the data. Increasing the number of levels in a layer over which a temperature lapse rate is calculated would lead to a greater likelihood that the temperature lapse rate (and the stability determined thereafter) accurately describes the real atmosphere – but this results in a larger departure from the theoretical stability class determined using the Pasquill stability scheme.

In order to determine if the type of stability has any impact on the results, a few additional checks are performed. First, the bias data are stratified by local time (obtained from Table 3 for each site) for the surface-100m layer in Table 13.

Table 13. Average Sfc-100m layer bias stratified by hour of the day, local time, for all sites and all times.

Hour	N	Bias	Std Bias	Abs(Bias)	Std Abs(Bias)
1am	2550	-0.7	0.9	0.8	0.7
2am	2404	-0.2	1.1	0.8	0.7
3am	2261	-0.6	0.9	0.8	0.7
6am	2749	-0.9	1.0	0.9	0.9
8am	2997	-0.8	1.5	1.3	1.0
11am	2901	-1.5	1.3	1.7	1.0
1pm	2574	0.9	1.3	1.3	0.8
2pm	2279	0.8	1.3	1.3	0.8
3pm	2361	-0.5	1.5	1.4	0.9
6pm	1657	-0.8	1.1	1.2	0.7
8pm	2503	0.8	1.5	1.3	1.1
11pm	1529	-0.7	0.9	0.9	0.7

For most times of day, the leading negative in front of the average bias indicates that the Pasquill stability scheme is outputting a class that is more unstable compared to the upper air stability class. AT 1pm, 2pm, and 8pm, a positive bias means that the scheme is predicting comparatively stable conditions. With absolute values of the bias maximized during the afternoon, in addition to larger standard deviations, the Pasquill stability scheme seems to perform worse during those times of day when unstable conditions would be most likely. A positive value for the average at 8pm is a source of confusion – but with larger values of standard deviation compared to the other evening hours, perhaps the day-to-night transition (when several different types of stability are possible), which would be occurring here, leads to an environment that the Pasquill stability scheme struggles to characterize.

Next, surface-100m layer data are stratified by the upper air stability – first for all six possible classes in Table 14, and then for just three possible types of stability (stable, unstable, or neutral) in Table 15.

Table 14. Average Sfc-100m layer bias stratified by upper air stability class, for all sites and all times.

Upper Air Stability Class	N	Bias	Std Bias	Abs(Bias)	Std Abs(Bias)
A (Extremely unstable)	1609	2.1	1.0	2.1	1.0
B (Moderately unstable)	3403	1.6	0.9	1.6	0.9
C (Slightly unstable)	2557	0.8	0.8	1.0	0.5
D (Neutral)	1057	-0.2	0.7	0.3	0.7
E (Slightly stable)	9923	-1.0	0.8	1.1	0.6
F (Moderately stable)	10216	-1.1	1.1	1.1	1.1

Table 15. Average Sfc-100m layer bias stratified by stability type, for all sites and all times.

Stability	N	Bias	Std Bias	Abs(Bias)	Std Abs(Bias)
Unstable	7569	1.4	1.0	1.5	0.9
Neutral	1057	-0.2	0.7	0.3	0.7
Stable	20139	-1.0	1.0	1.1	0.9

Tables 14 and 15 show that the bias is closest to zero for neutral conditions, with lower values of standard deviation suggesting that the Pasquill stability scheme performs comparatively better for neutral stability. The bias becomes increasingly positive and negative for unstable and stable conditions, respectively – with a greater magnitude in the bias and a lower standard deviation for unstable conditions than for stable conditions. This would indicate that, when true stability is unstable, the Pasquill scheme tends towards a more stable category than what is observed – and the scheme tends towards a more unstable category when the true stability is stable. This is in agreement with some of the results from Table 13, which indicated

that the Pasquill stability scheme trended more stable for those times usually corresponding to unstable conditions. The results from Tables 14 and 15 for stable conditions are also somewhat in agreement with previous results – when considering that a stable category was determined for most of the observations (over 20,000 of them). Under these conditions, the Pasquill stability scheme usually trended slightly more unstable compared to the upper air stability category.

Finally, in order to assess the performance of individual Pasquill stability classes, the number of occurrences of an unstable, stable, or neutral stability category (determined using the temperature lapse rate) is stratified by the Pasquill stability category determined for the co-located surface data. Data for the surface-100m layer is shown in Table 16.

Table 16. Percentage of the total number of instances of each Pasquill stability class for which the temperature lapse rate determined Unstable, Stable, or Neutral stability.

Pasquill stability	N Pclass	Unstable		Stable		Neutral	
A	230	171	74.3%	57	24.8%	2	0.9%
B	1934	1111	57.4%	747	38.6%	76	3.9%
C	2490	1367	54.9%	1005	40.4%	118	4.7%
D	16512	4587	27.8%	11123	67.4%	802	4.9%
E	2286	176	7.7%	2075	90.8%	35	1.5%
F	5313	157	3.0%	5132	96.6%	24	0.5%

While Tables 14 and 15 indicated that while stable stability is determined for most of the cases, the Pasquill stability scheme predicted neutral stability for more than half of all the cases. However, the actual stability was neutral in less than five percent of the cases for which a Pasquill class of D was determined. Stable conditions were usually occurring when the neutral class was chosen, but it should be noted that the Pasquill stability scheme did correctly predict neutral stability for most of the cases where neutral conditions were actually present. The two stable classes performed the best of all six classes, with over 90% of all the class E and F cases actually occurring in stable conditions – however, just over half of the cases where the upper air

stability is found to be stable also have a Pasquill stability class of E or F. Around 74% of the class A cases actually occurred under unstable conditions, but only between 50-60% of the class B and class C cases actually occurred under unstable conditions – around 40% of the cases for each class actually occurred under stable conditions.

The large prevalence of the neutral case may result from a combination of several factors. First, the neutral category is always determined under overcast skies, and is usually chosen when wind speeds are greater than 6m/s during the day or night. However, cloudy skies and stronger wind speeds may not always equate to neutral stability. Such conditions are common in the vicinity of frontal boundaries, for example, but precipitation and convection initiation along these features indicates that vertical motion is still occurring. A bias toward neutral conditions in the Pasquill scheme may also result, in part, from the fact that a stable Pasquill category cannot be chosen during the day. Another examination of the the lapse rate histograms at 12z for Merignac and Kiev (Figures 10 and 11, bottom), a time which corresponds to the early afternoon for both sites, reveals that temperature lapse rates indicating stable conditions can actually occur during the day, if infrequently. However, meteorological phenomena commonly found in stable conditions, such as stratiform clouds, may correspond to Pasquill class D during the day or night.

The success of the classes under stable conditions is perhaps unsurprising. In spite of an effort to include numerous types of stability in the dataset, a large bias toward stable conditions exists in the upper air data, and this may have ended up working in favor of the Pasquill stability scheme. This bias may result from the choice of sites or the depth of the layers over which the temperature lapse rates were calculated, but it should also be noted that only the dry adiabatic lapse rate, and never the saturated adiabatic lapse rate, was used to categorize the upper air data. Therefore, a temperature lapse rate around $7℃/km$, for example, would meet "stable" stability

criteria in this study, when in reality this lapse rate may correspond to stable or unstable conditions depending on whether the air is found to be saturated.

IV. Conclusion

Stability determined via the Pasquill stability classification scheme has been tested against stability classes determined using temperature lapse rates, defined as the true stability. On average, the Pasquill classes were found to stray from the true stability by one class – but larger errors are possible especially in the warmer months, when more daylight allows some sites to experience a wider range of stabilities than in the winter. While other factors such as the number of levels in the soundings over which temperature lapse rates were calculated seemed to have a slight impact on the difference between the Pasquill and upper air stability estimates, it seems that the most important factor determining how well the Pasquill scheme performs is the conditions that govern the choice of the Pasquill class. The scheme was biased towards predicting neutral conditions – with the result that neutral conditions actually occurred for only a very small percentage of the cases when Pasquill stability class D was determined. Otherwise, the scheme over-predicted neutral conditions particularly when the actual stability is "stable". The scheme performed very well when stable conditions were present, with over 90% of the E and F classes having found to occur under actual stable conditions – however, it is unclear the role that a stable bias in the temperature data plays in this.

Earlier studies have presented evidence indicating that other methods of determining the rate of diffusion often result in more accurate pollutant concentrations than the Pasquill scheme. This alone might give one pause before attempting to apply the Pasquill method for other purposes, since the scheme seems to underperform even when it is used for diffusion purposes. Additional work may need to be done to determine if a stable bias in the temperature lapse rate dataset had any impact on the results, and a way to accomplish this may be to obtain data from additional sites where soundings are launched during the afternoon and early evening.

Additionally, calculating the temperature lapse rates over a layer shallower than sfc-100m, and allowing for the consideration of moisture, may help to cut down on the stable bias. However, the results presented here indicate that the Pasquill scheme is most useful only under certain stability conditions, so implementing this method in order to characterize the overall stability may prove problematic.

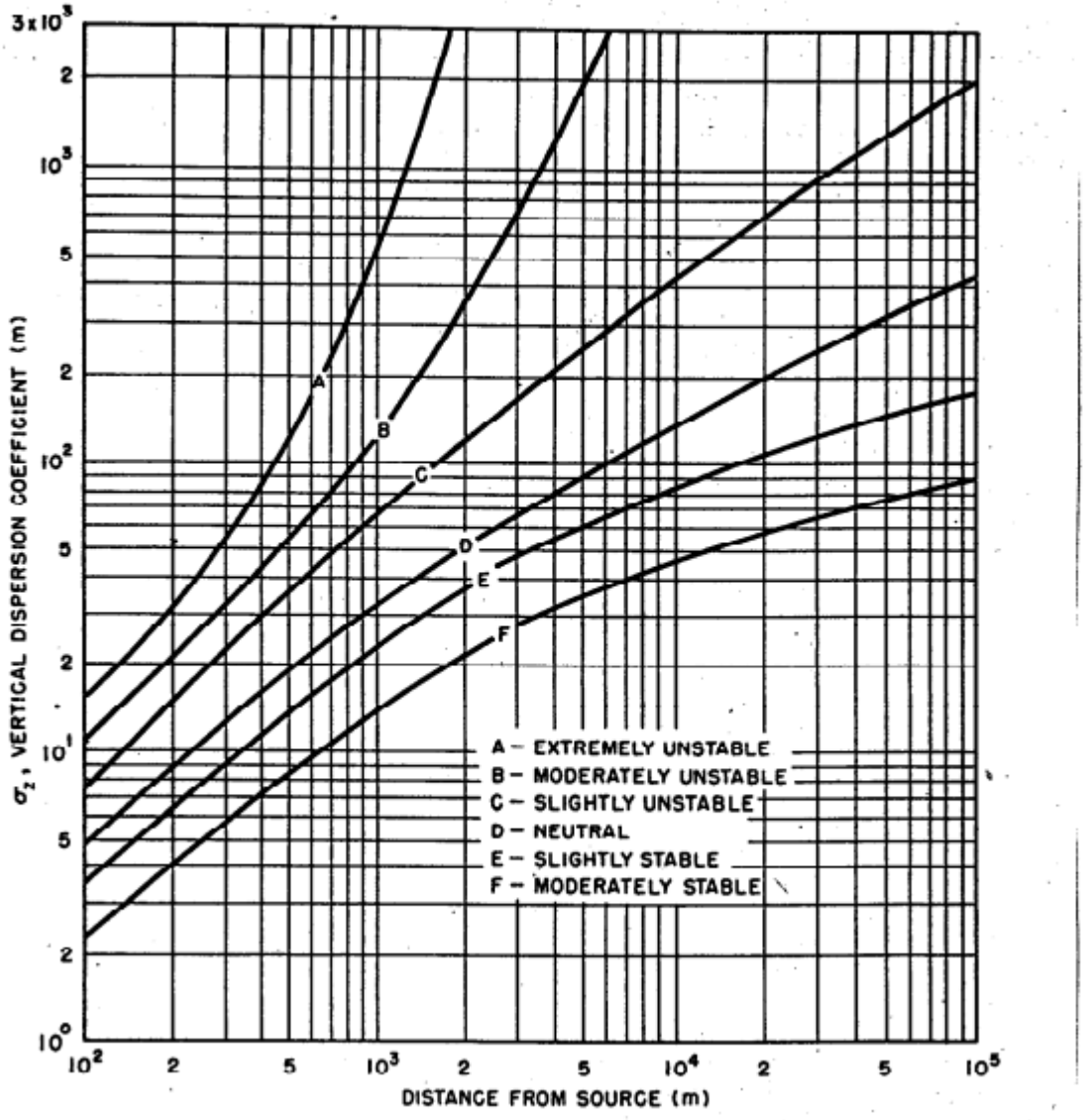

Figure 1: Relationship between the vertical standard deviation of pollution concentration and the distance from the source. From Pasquill (1961).

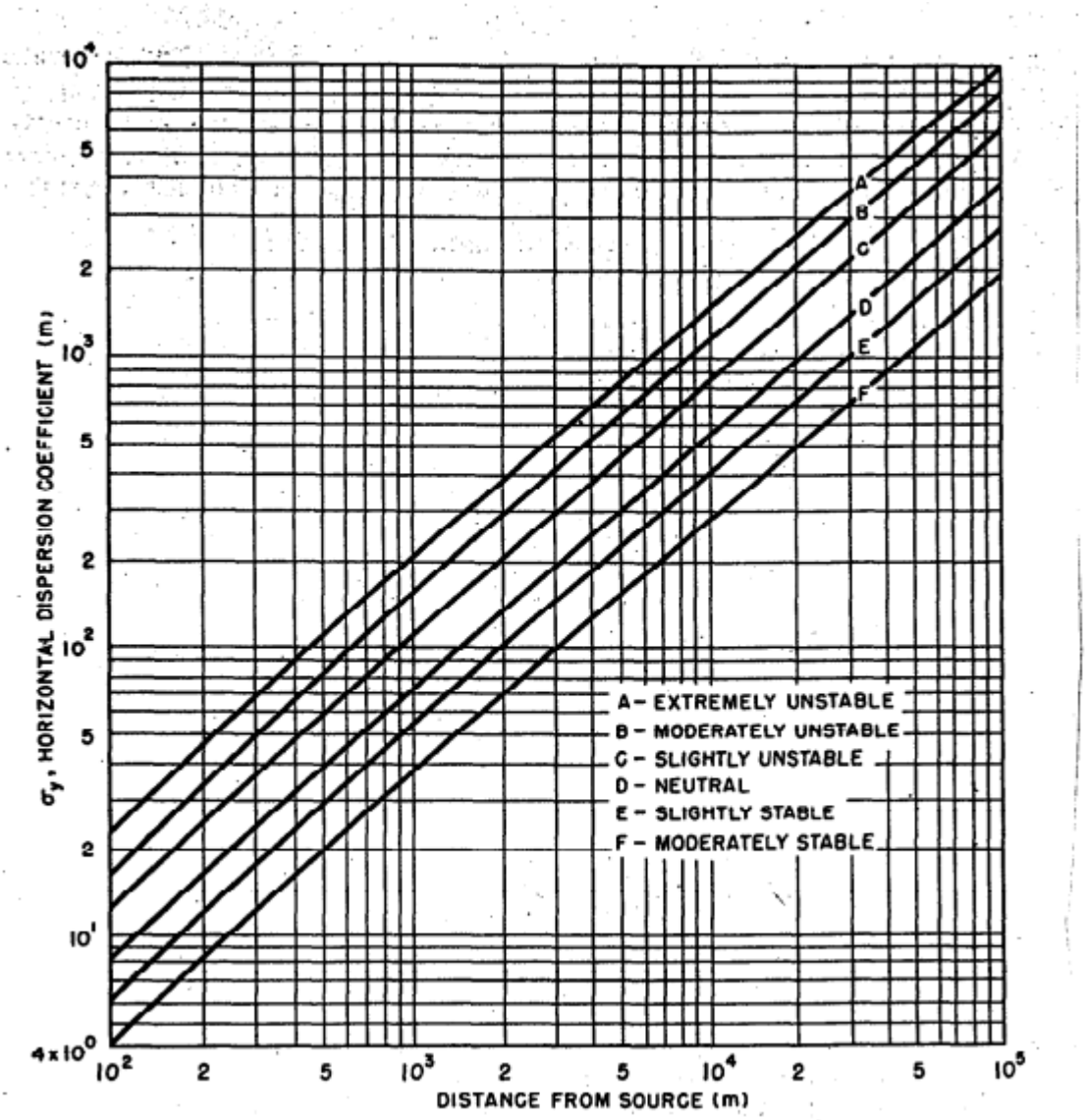

Figure 2: Relationship between the horizontal standard deviation of a pollutant concentration and the distance from the source. From Pasquill (1961).

Figure 3. Map of Europe and Asia. Sites are indicated with blue markers.

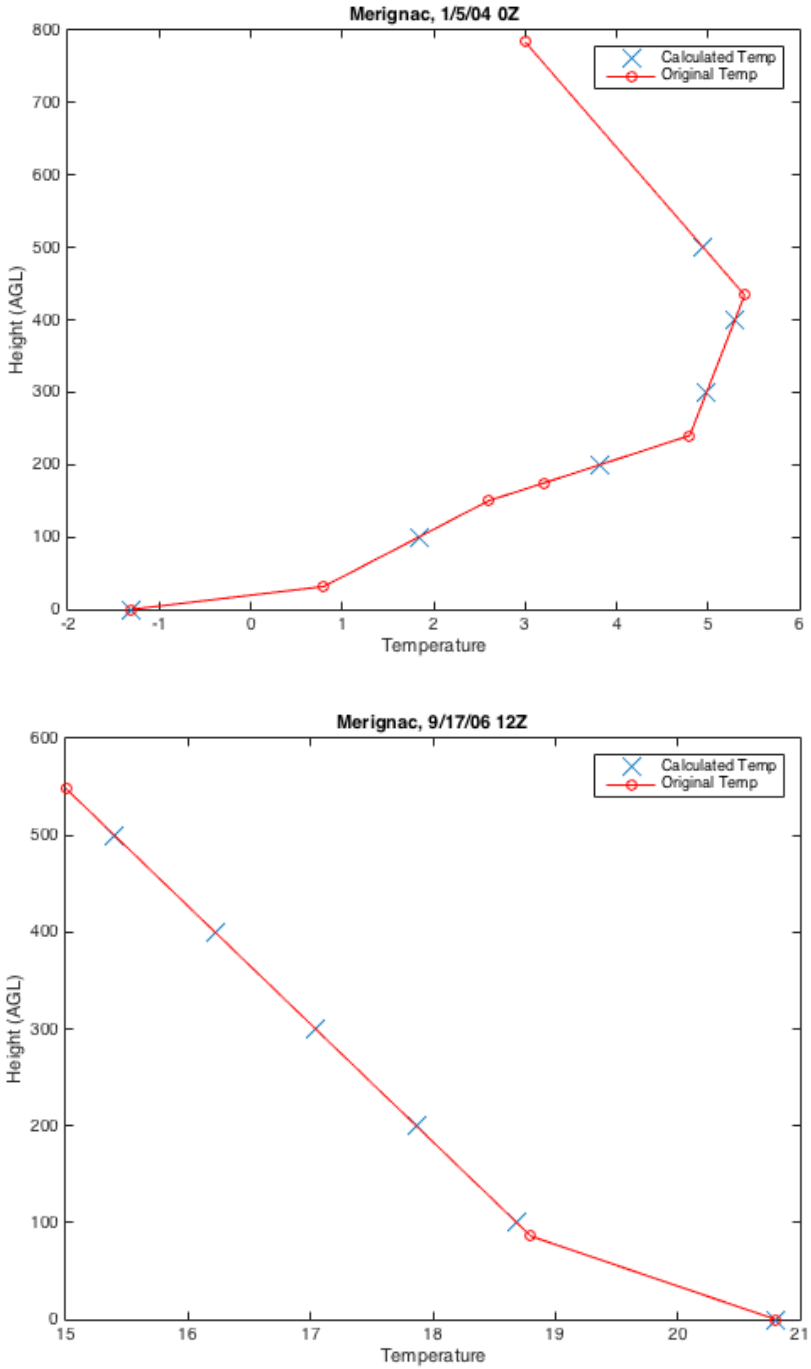

Figure 4. Sample soundings from a 0z (top) and 12z (bottom) observation for Merignac, France. The red line denotes the original temperature trace. The red circles are the original temperatures that make up the trace, and the blue crosses are the sfc-500m temperatures. Blue crosses co-located with red circles indicate that the temperature was already present in the original sounding. Blue crosses along the temperature trace, but not overlapping with red circles, indicate that the temperature at that level was calculated.

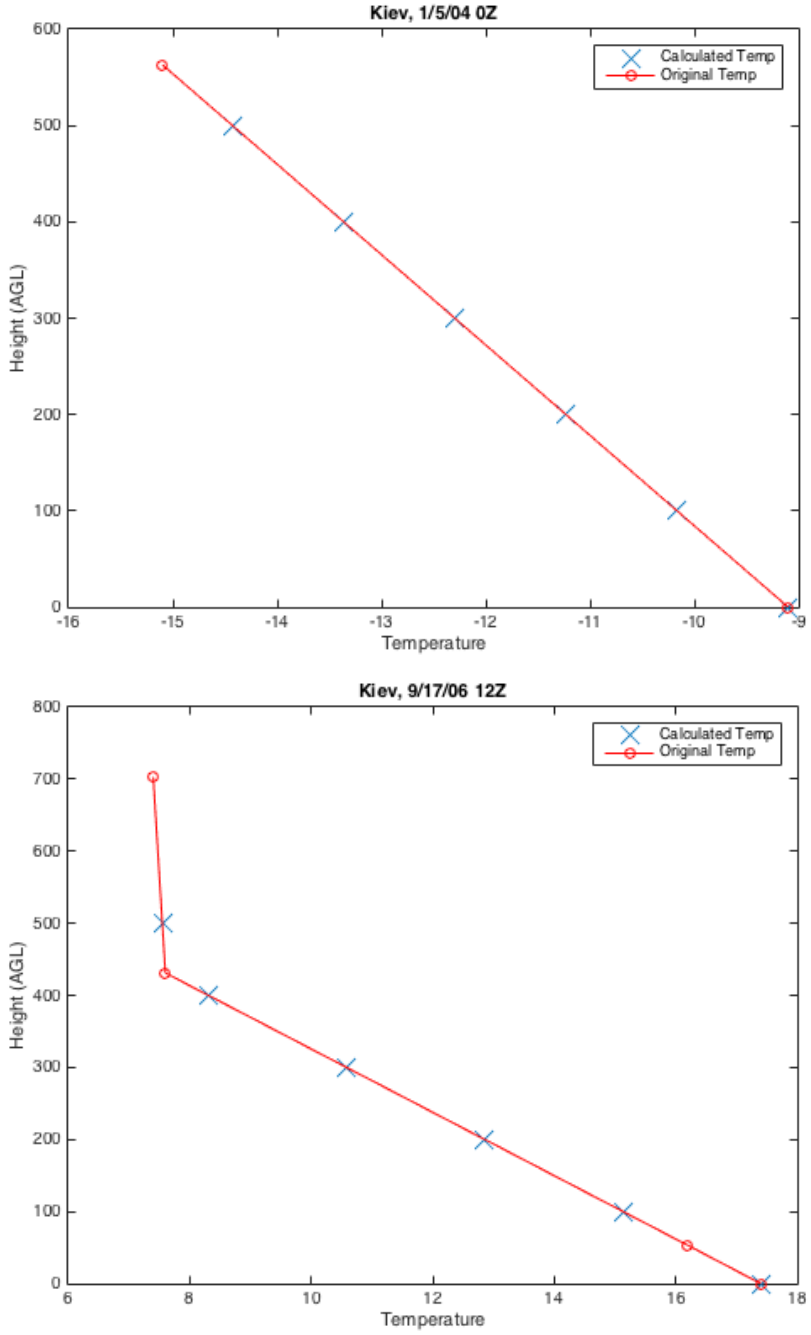

Figure 5. Same as figure 4, but for Kiev, UA.

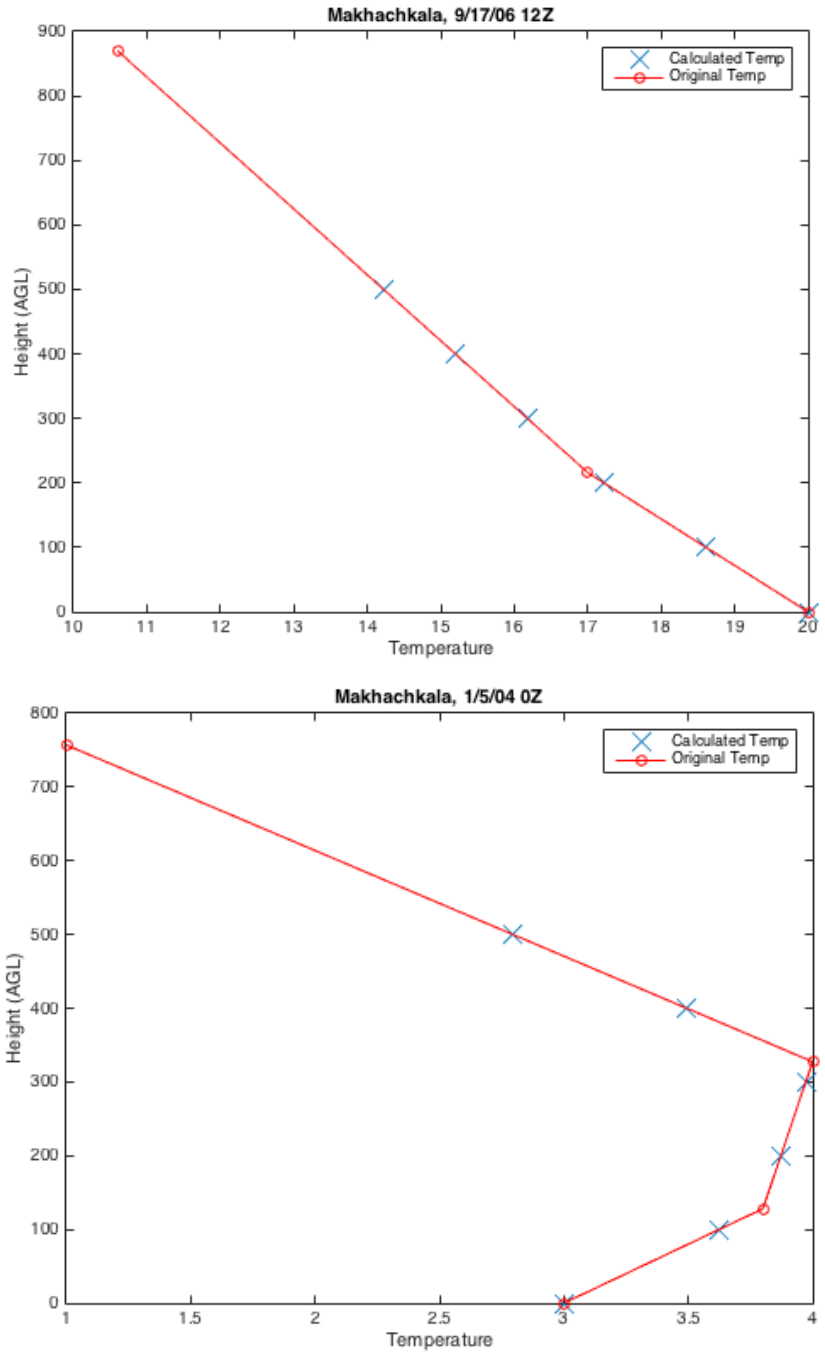

Figure 6. Same as Figure 4, for Makhachkala, RS.

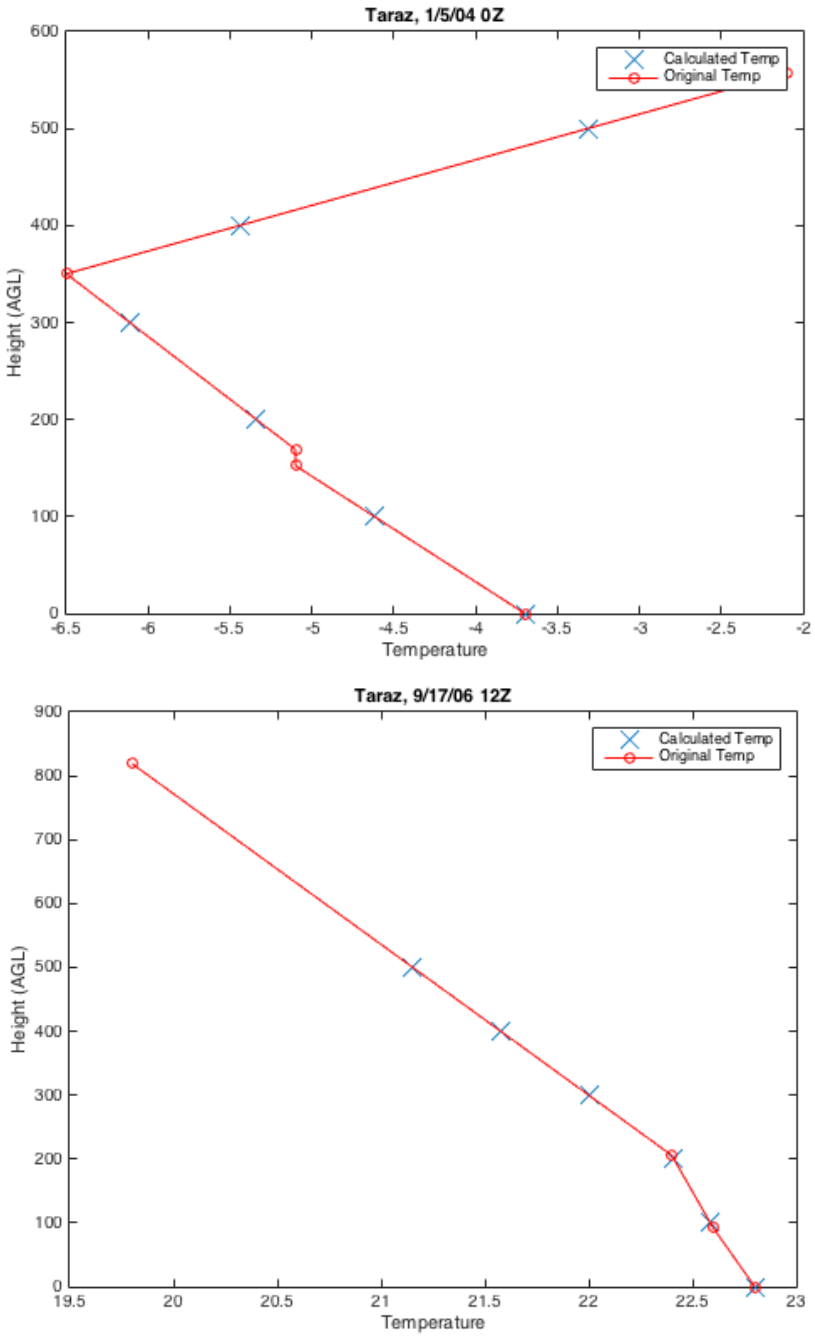

Figure 7. Same as Figure 4, but for Taraz, KZ.

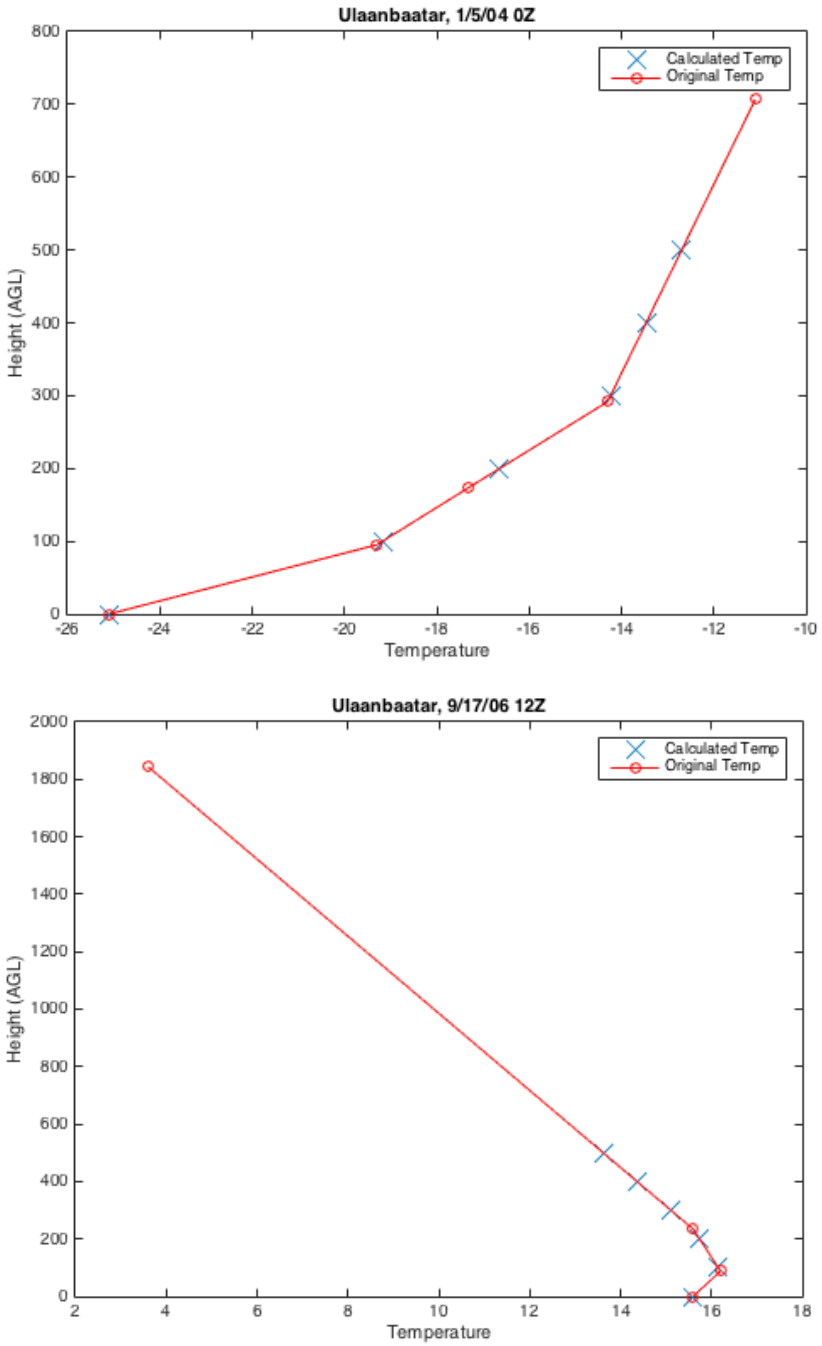

Figure 8. Same as Figure 4, but for Ulaanbaatar, MN.

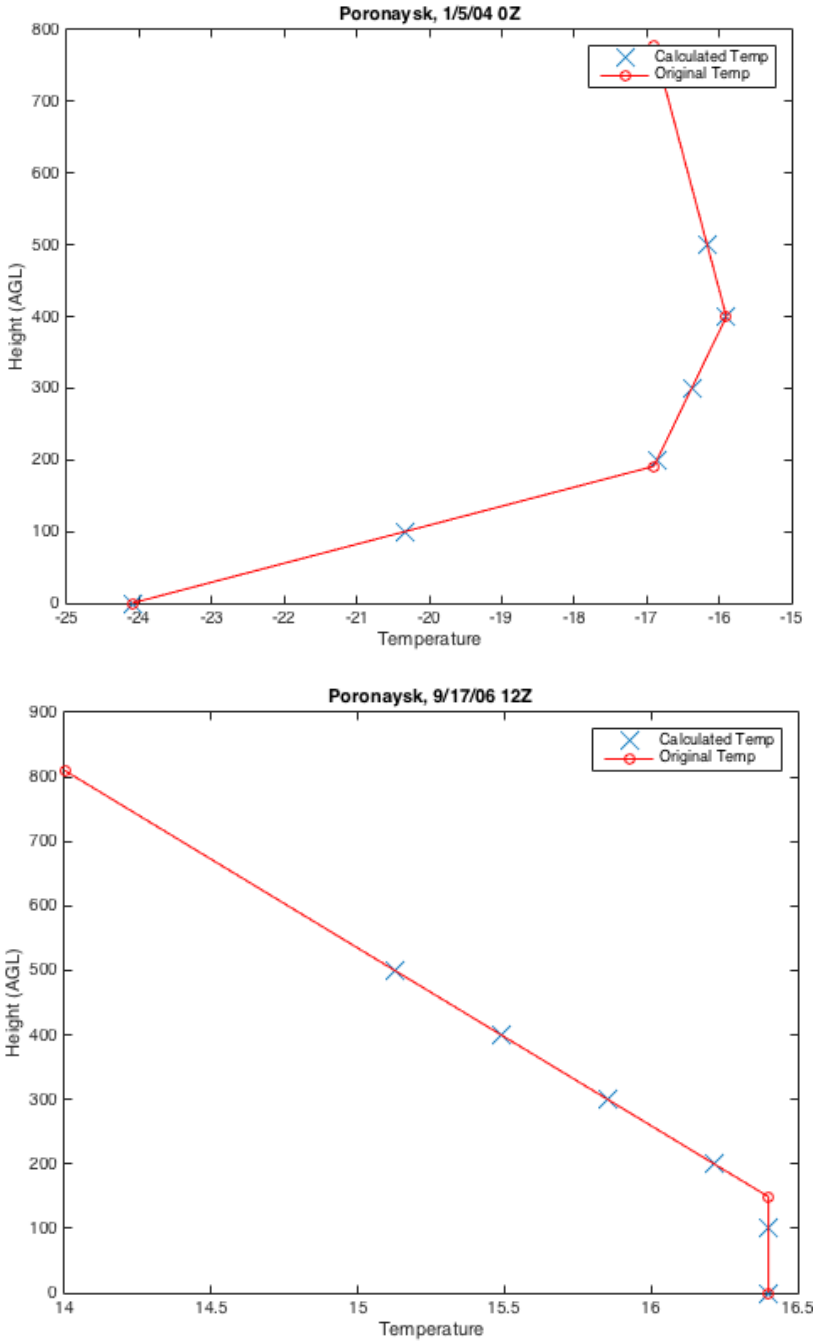

Figure 9. Same as Figure 4, but for Poronaysk, RS.

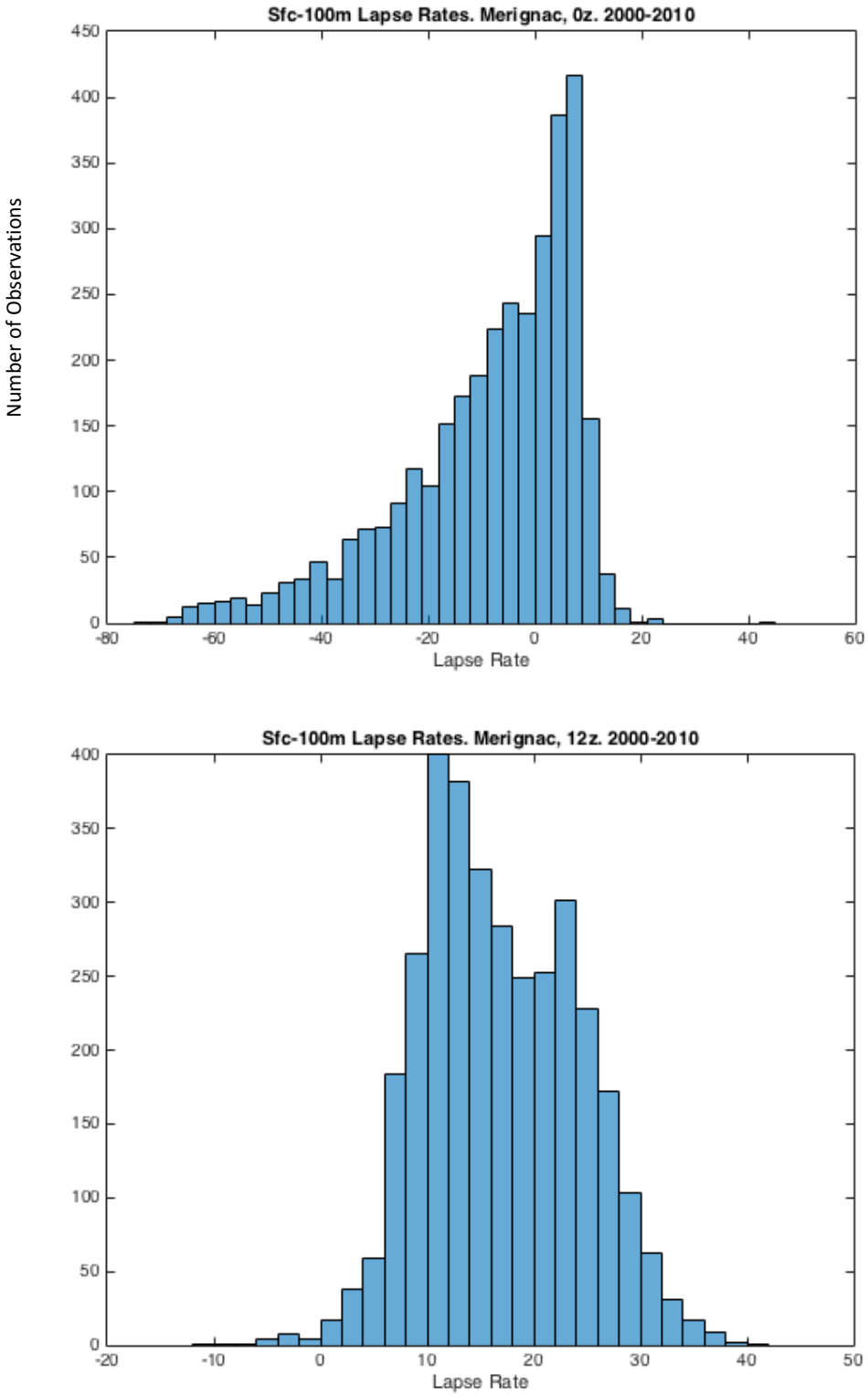

Figure 10. Histograms of the surface-100m layer lapse rates for Merignac, FR at 0z (top) and 12z (bottom) for the years 2000-2010.

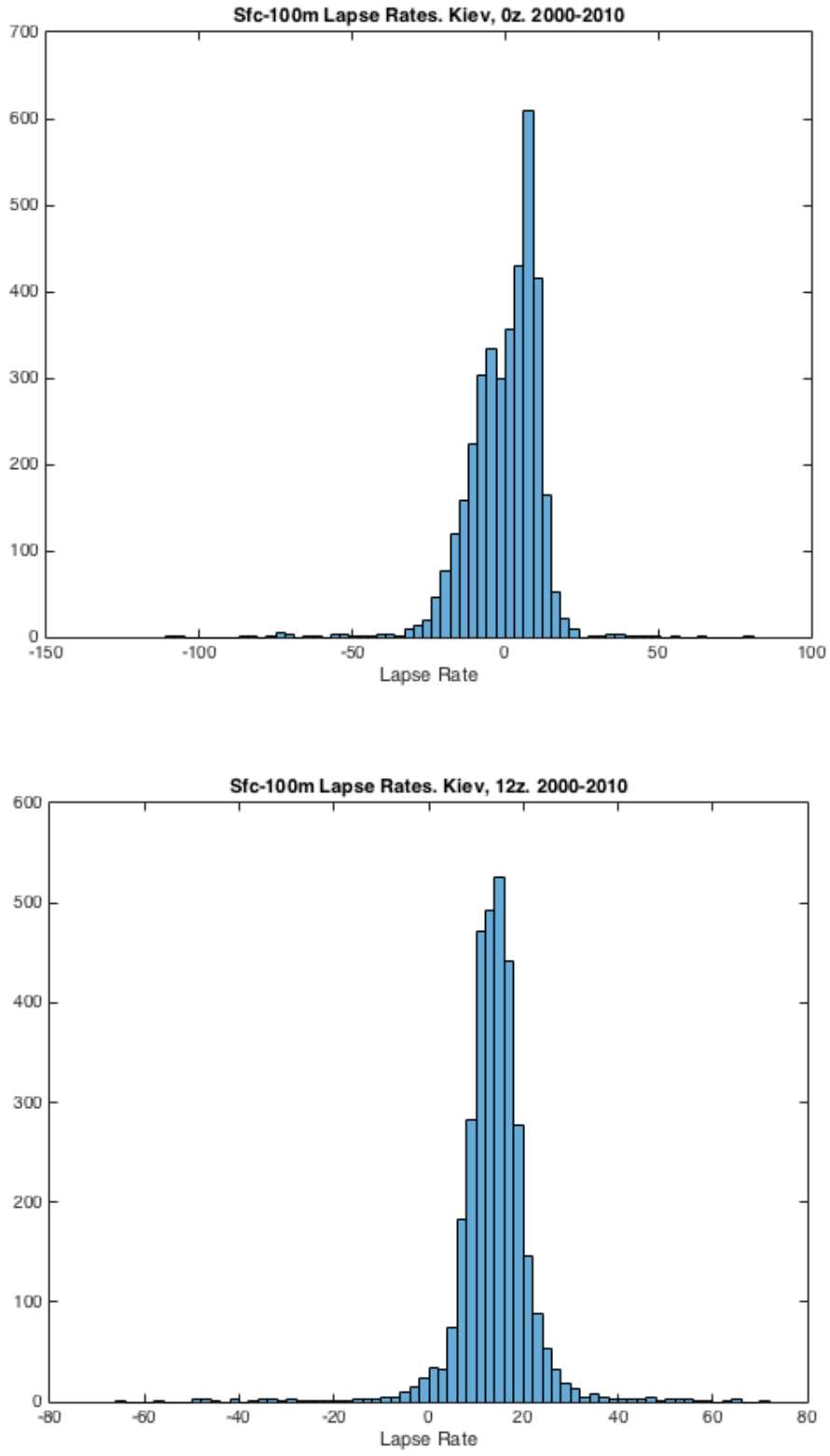

Figure 11. Histograms of the surface-100m layer lapse rates for Kiev, UA at 0z (top) and 12z (bottom) for the years 2000-2010.

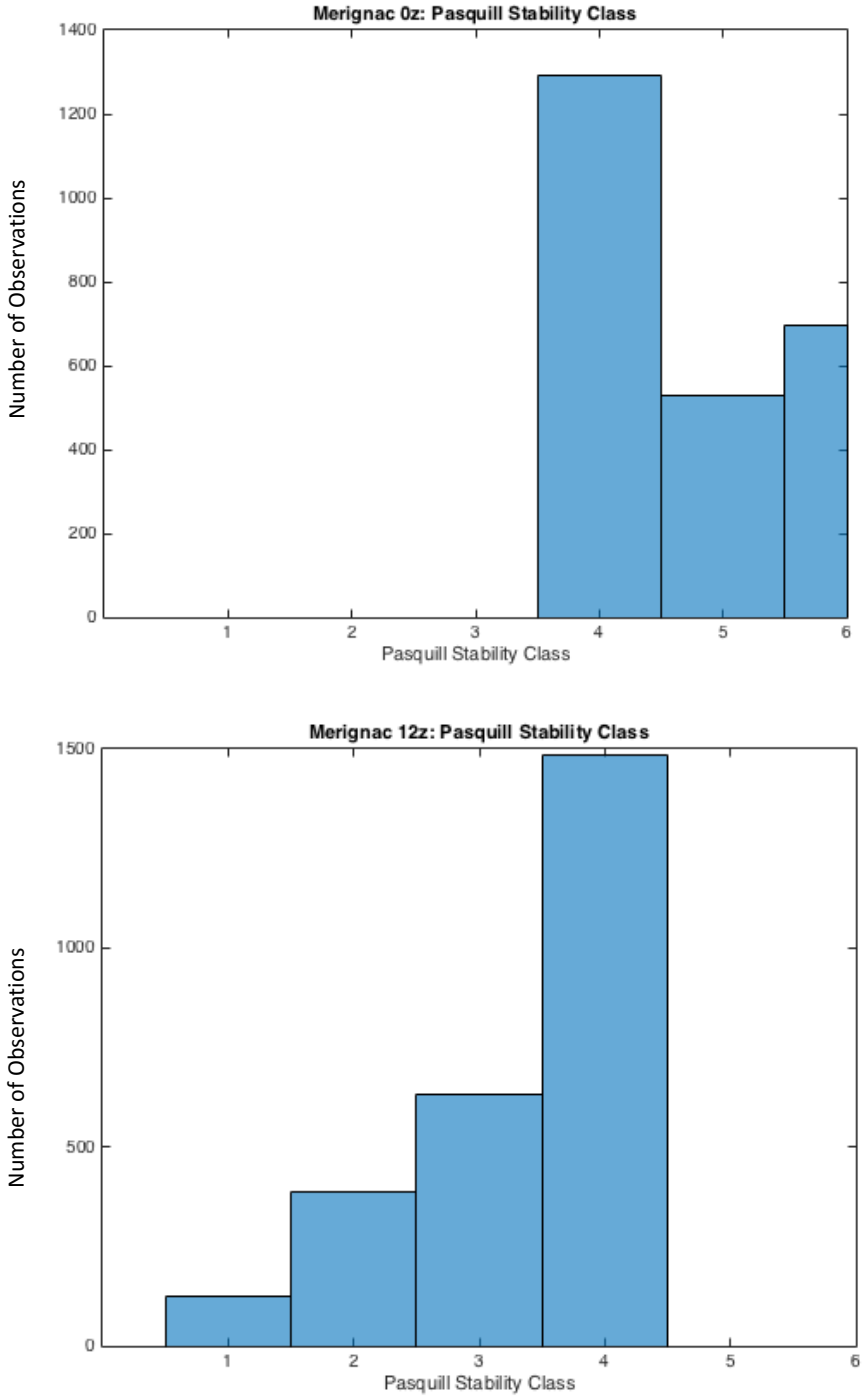

Figure 12. Histograms of Pasquill Stability Class determined for Merignac, FR for 0z (top) and 12z (bottom).

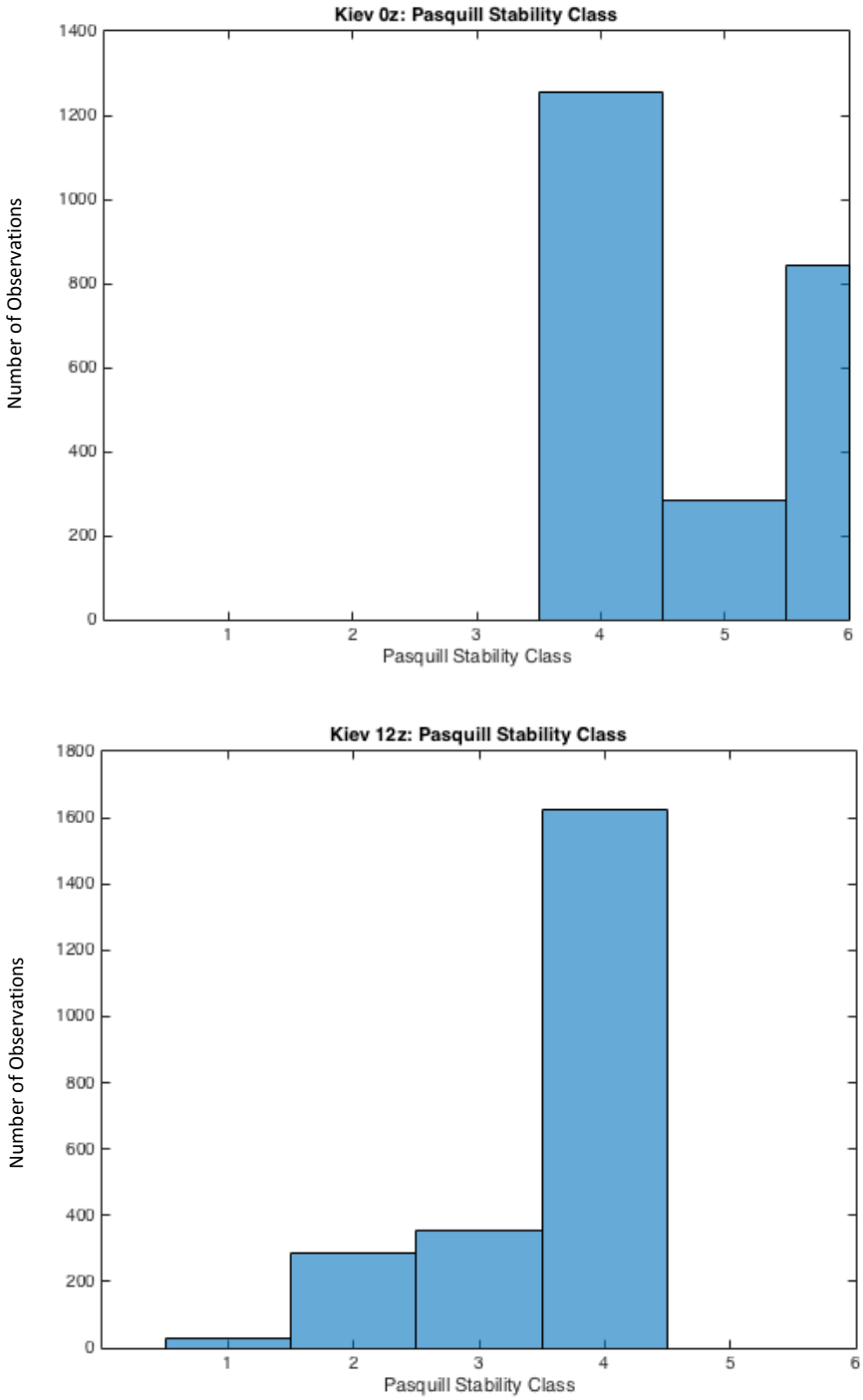

Figure 13. Same as Figure 12, but for Kiev UA

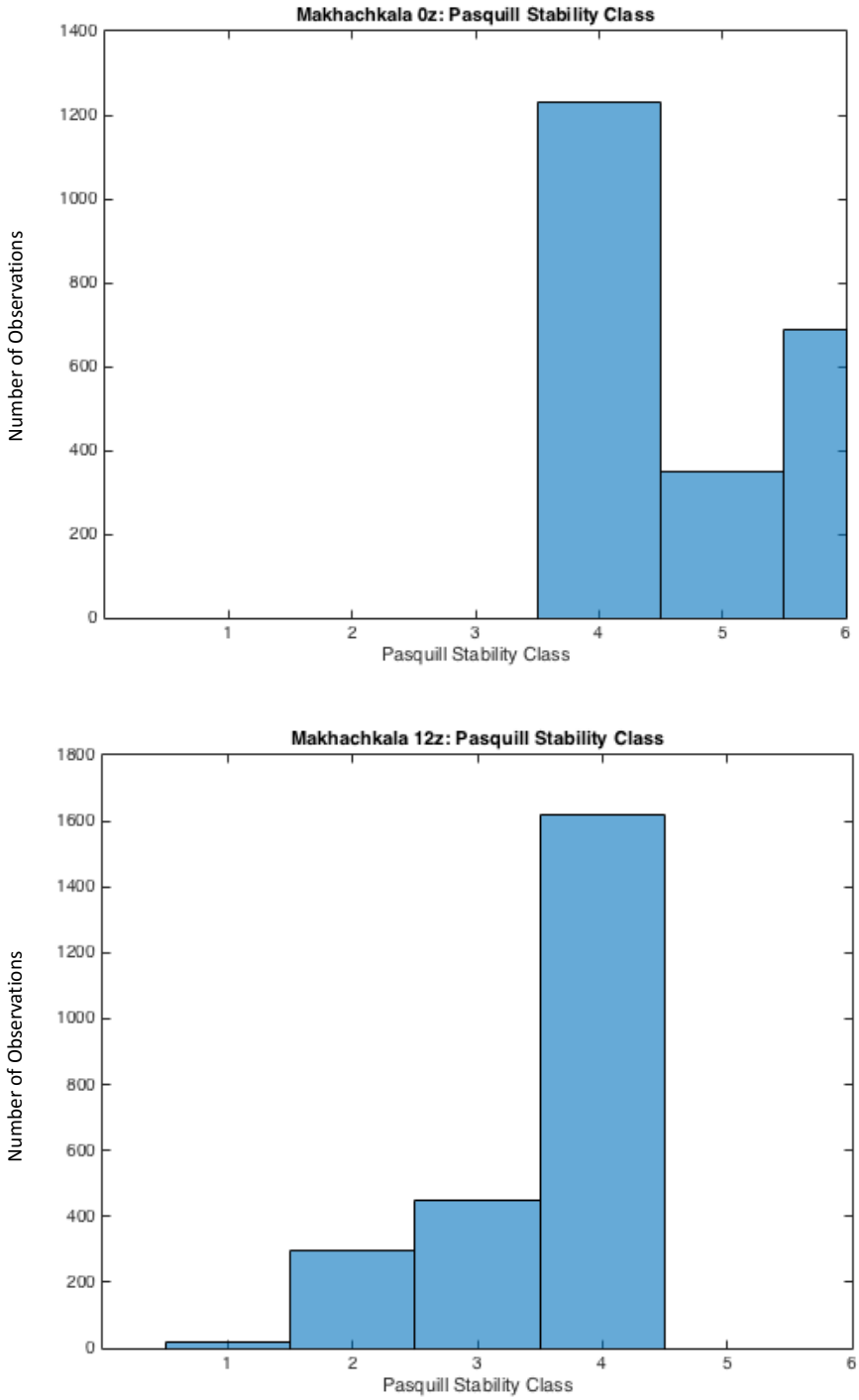

Figure 14. Same as Figure 12, but for Makhachkala, RS.

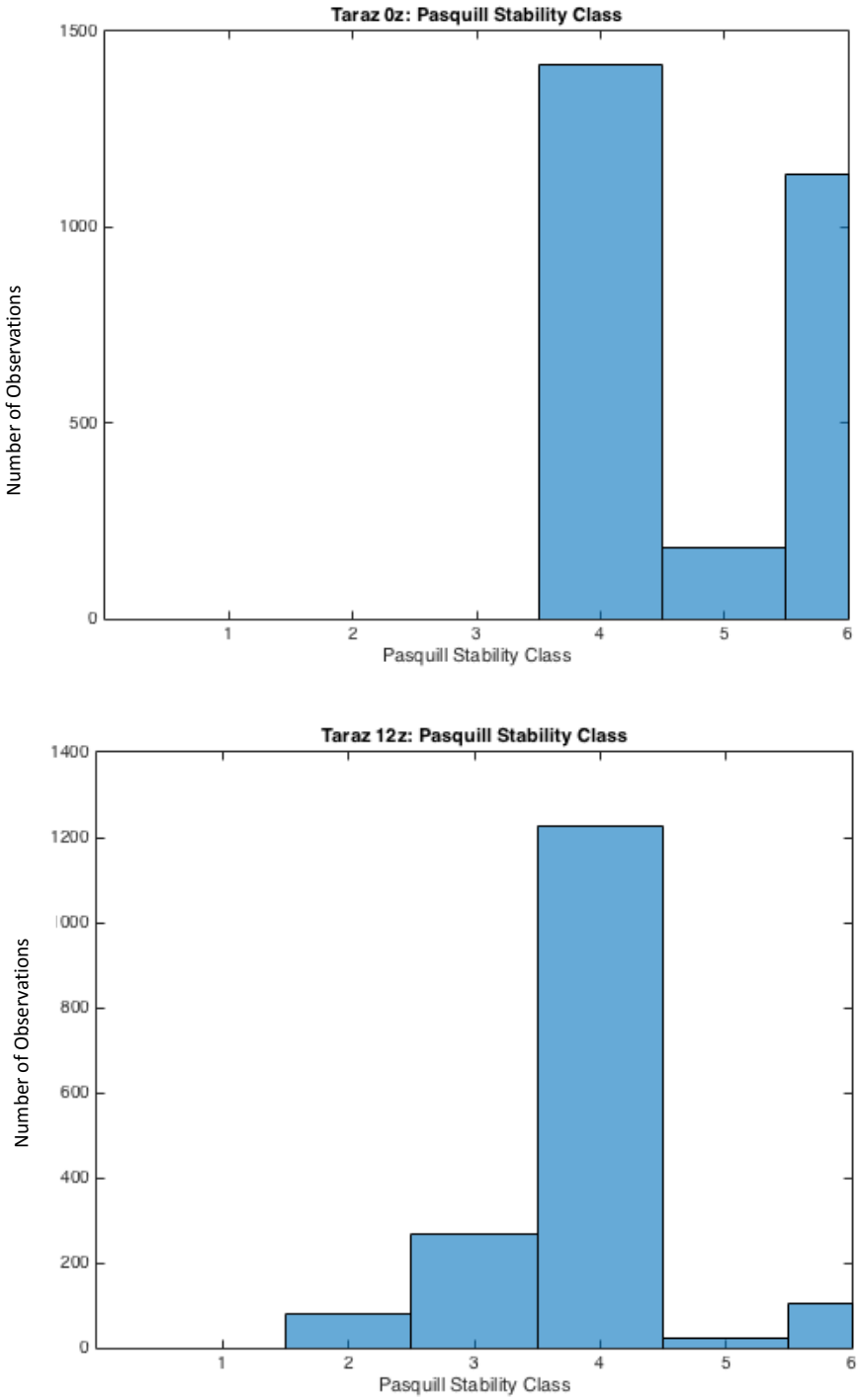

Figure 15. Same as Figure 12, but for Taraz, KZ.

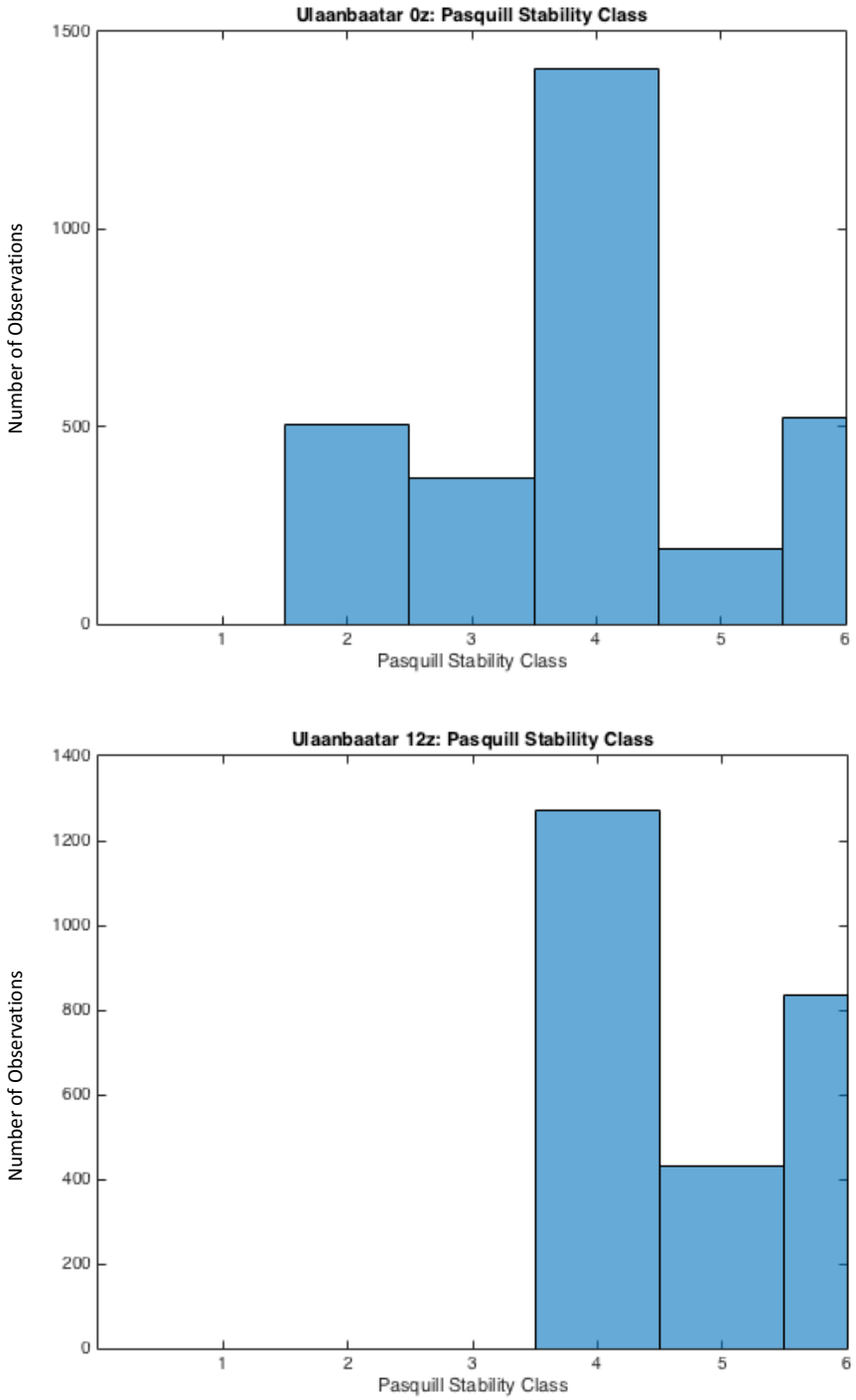

Figure 16. Same as Figure 12, but for Ulaanbaatar, MN.

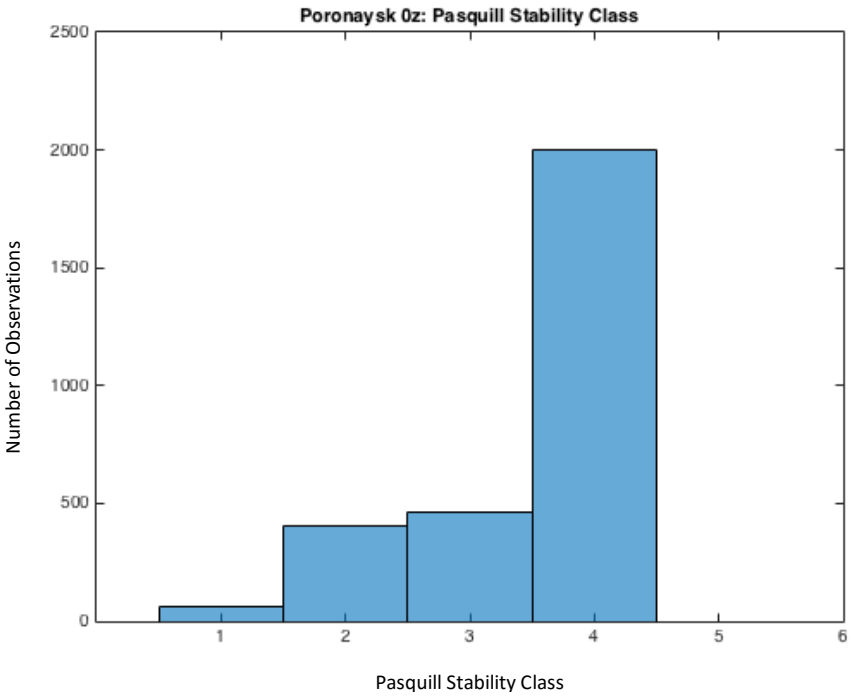

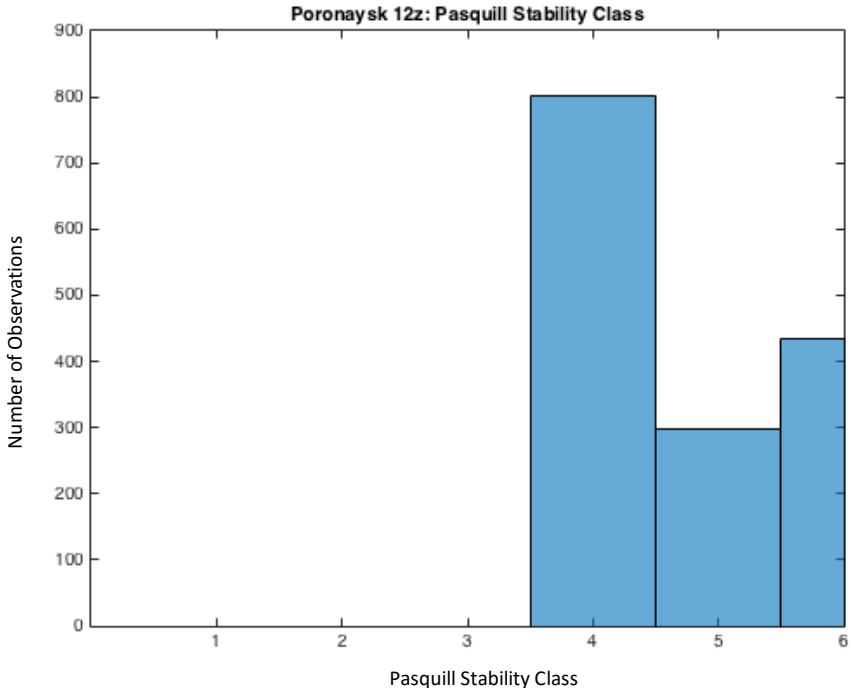

Figure 17. Same as Figure 12, but for Poronaysk, RS.

Works Cited

Chapman, Lee, John E Thornes and Andrew V Bradley. "Modelling of road surface temperature from a geographical parameter database. Part 1: Statistical". *Meteorol. Appl.* 8 (2001): 409 – 419.

Chambers, et al. "On the Use of Radon for Quantifying the Effects of Atmospheric Stability on Urban Emissions". *Atmospheric Chemistry and Physics* 15, no 3 (2015): 1174 – 1190.

Crawford, et al. "Assessing the impact of Atmospheric Stability on Locally and Remotely Sourced Aerosols at Richmond, Australia, Using Radon-222". *Atmospheric Environment* 127 (2016): 107 – 117.

Duenas, C. et al. "Disequilibrium of Radon and its Short-Lived Daughters near the Ground with Atmospheric Stability". *Journal of Geophysical Research – Atmospheres* 99, no D6 (1994): 12865 – 12872.

Erbrink, HJ and RDA Scholten. "Atmospheric Turbulence above Coastal Waters – Determination of Stability Classes and a Simple Model for Offshore Flow including Advection and Dissipation". *Journal of Applied Meteorology* 34, no 10 (1995): 2278 – 2293.

Handler, F.A. and Jason M. Edmonds. "Quantitative Analysis of Effects of UV Exposure and Spore Cluster Size on Deposition and Inhalation Hazards of Bacillus Spores". *Aerosol Science and Technology* 49, no 11 (2015): 1121 – 1130.

Hanna, S.R., Egan, B.A., and J. Purdum. "Evaluation of the ADMS, AERMOD, and ISC3 dispersion models with the OPTEX, Duke Forest, Kincaid, Indianapolis, and Lovett field datasets." *International Journal of Environment and Pollution* 16, no 1-6 (2001): 301-314.

Kim, Hee-Jong, Ill-Hee Yoon, Byung-Hyuk Kwon, and Man-Chun Heo. "Characteristic of the Nocturnal Inversion Layer observed by Tethersonde in Daegu". *Journal of Environmental Science International* 11, no 3 (2002).

Keohn, A.C., A.B. Leytem, D.L. Bjorneberg. "Comparison of Atmospheric Stability Methods for Calculating Ammonia and Methane Emission Rates with Windtrax". *Transactions of the Asabe*56, no 2 (2013): 763 – 768.

Krueger, Eduardo and Rohinton Emmanuel. "Accounting for atmospheric stability conditions in urban heat island studies: The case of Glasgow, UK." *Landscape and Urban Planning* 117 (2013): 112 – 121.

Kurzeja, R.J., S. Berman, and A.H. Weber. "A Climatological Study of the Nocturnal Planetary Boundary Layer". *Boundary Layer Meteorology* 54, no 1 – 2 (1991): 105 – 128.

Leatherdale, Duncan. "Windscale Piles: Cockroft's Follies Avoided Nuclear Disaster." *BBC News*. 4 November 2014.

Luna, R. E. and H. W. Church. " A Comparison of Turbulence Intensity and Stability Ratio Measurements to Pasquill Stability Classes." *Journal of Applied Meteorology* 11 (1972): 663–669.

Masters, et al. " Toward Objective, Standardized Intensity Estimates from Surface Wind Speed Observations." *Bulletin of the American Meteorological Society* (2010): 1665-1681.

Mohan, M. and T.A. Siddiqui. "Analysis of Various Schemes for the Estimation of Atmospheric Stability Classification." *Atmospheric Environment* 32, no 21 (1998): 3775 – 3781.

Mohan, Manju, Yukihiro Kikegawa, B. R. Gurjar, Shweta Bhati, Anurag Kandya, and Koichi Ogawa. "Urban Heat Island Assessment for a Tropical Urban Airshed in India". *Atmospheric and Climate Sciences* 2, no. 2 (2012).

No, Sang-Tae and Kang-Soo Kim. “Analysis of the Thermal Performance of Curtain Walls in High-Rise Residential Buildings”. *Journal of Asian Architecture and Building Engineering*, November 2005.

Pasqill, F. and F. B. Smith. *Atmospheric Diffusion: Study of the Dispersion of Windborne Material from Industrial and Other Sources*. Chichester: Ellis Horwood Limited, 1983.

Pasquill, F. “The Estimation of the Dispersion of Windborne Material.” *Meteorological Magazine* 90 (1961): 33 – 49.

Sempreviva, A.M., A. Lavagnini, V. Quesada. “Experimental Test of the EEC Wind Climatology Model in a Mediterranean Coastal Area”. *Nuovo Cimento Della Societa Italiana di Fisica C – Geophysics and Space Physics* 17, no 5 (1994).

Serizawa, Y., E. Ohba, and Y. Watanabe. “Radio Meteorological Analysis for Forecasting Microwave Fading Occurrence”. *IEEE Transactions on Power Delivery* 7, no 4 (1992): 1754 – 1759.

Stull, Roland. *An Introduction to Boundary Layer Meteorology*. Kluwer Academic Publishers, 1950.

Tomlinson, C. J. et al. “Derivation of Birmingham's Summer Surface Urban Heat Island from MODIS Satellite Images.” *International Journal of Climatology* 32 (2012): 214 – 224.

Turner, D. Bruce. “A Diffusion Model for an Urban Area.” *Journal of Applied Meteorology* 3 (1964): 83–91.

Van den Berg, G.P. “Effects of the Wind Profile at Night on Wind Turbine Sound.” *Journal of Sound and Vibration* 277 (2004): 955 – 970.

Van den Berg, G.P. “The Beat is Getting Stronger: The Effect of Atmospheric Stability on Low Frequency Modulated Sound of Wind Turbines.” *Noise Notes* 4, no 4 (2005): 15 – 40.

Wang, J.M. “Turbulence Characteristics in an Urban Atmosphere of Complex Terrain”. *Atmospheric Environment Part A – General Topics* 26, no 15 (1992): 2717 – 2724.